

February 8, 2020

hep-ph/01xxx

# Complete next-to-leading order QCD corrections to charged Higgs boson associated production with top quark at the CERN Large Hadron Collider

SHOU-HUA ZHU

*Institut für Theoretische Physik, Universität Karlsruhe,  
D-76128 Karlsruhe, Germany*

The complete next-to-leading order (NLO) QCD corrections to charged Higgs boson associated production with top quark through  $bg \rightarrow tH^-$  at the CERN Large Hadron Collider are calculated in the minimal supersymmetric standard model (MSSM) and two-Higgs-doublet model in the  $\overline{MS}$  scheme. The NLO QCD corrections can reduce the scales dependence compared to that at tree level, and the K-factor varies from  $\sim 1.55$  to  $\sim 1.75$  when charged Higgs mass increases from 180 GeV to 1000 GeV.

PACS number: 12.60.Jv, 12.15.Lk, 14.80.Cp, 14.70.Fm

## I. INTRODUCTION

The detection of Higgs particles is one of the most important objectives of the Large Hadron Collider (LHC). Charged Higgs bosons are predicted in extended versions of the Standard model (SM), like two-Higgs-doublet models (2HDM) and the Minimal Supersymmetric Standard Model (MSSM). Unlike the neutral Higgs boson, a discovery of such an additional charged Higgs boson will immediately indicate physics beyond the SM; there is, hence, strong theoretical and experimental activity to provide the basis for its accurate exploration.

At hadron colliders, the charged Higgs boson  $H^\pm$  could appear as the decay product of primarily produced top quarks if the mass of  $H^\pm$  is smaller than  $m_t - m_b$ . For heavier  $H^\pm$ , the direct production mechanism for  $H^\pm$  production have been investigated. At the LHC, the primary charged Higgs boson production channel is the single Higgs-boson production associated with heavy quark,  $gb \rightarrow H^\pm t$  [1] \*. The study [3,4] shows that this process can explore the parameter space for  $m_{H^\pm} > 1TeV$  and  $\tan\beta$  down to at least  $\sim 3$ , and potentially to  $\sim 1.5$ . Therefore, it is necessary to calculate and implement also the loop contributions to  $gb \rightarrow H^\pm t$  for more accurate theoretical predictions.

In literature, part of the NLO QCD corrections to  $gb \rightarrow H^\pm t$ , the initial-gluon contribution of  $gg \rightarrow H^\pm t\bar{b}$  has been calculated [5]. The supersymmetric electroweak corrections arising from the quantum effects which are induced by potentially large Yukawa couplings from the Higgs sector and the chargino-top(bottom)-sbottom(stop) couplings, neutralino-top(bottom)-stop(sbottom) couplings and charged Higgs-stop-sbottom couplings are also studied [1,6], which can give rise to a 15% reduction of the lowest-order result. In Ref. [7], the electro-weak corrections to the process are also discussed. In this paper, we deal with the complete next-to-leading order QCD corrections to  $gb \rightarrow H^\pm t$ .

The arrangement of this paper is as follows. Section II contains the analytic results, and in Section III we present numerical examples and discuss the implications of our results. The lengthy expressions of the form factors are collected in the Appendix.

---

\* See Ref. [2] for other charged Higgs boson production mechanism.

## II. ANALYTIC EXPRESSIONS

Including the NLO QCD corrections, the cross sections for  $PP \rightarrow tH^-X$  at the CERN LHC can be written as

$$\sigma = \sigma^{Born} + \sigma^{Vir} + \sigma^{Real}, \quad (1)$$

where  $\sigma^{Born}$  is the cross section at Born level,  $\sigma^{Vir}$  and  $\sigma^{Real}$  are contributions from virtual and real corrections.

### A. Born level

The Feynman diagrams for the charged Higgs boson production via  $b(p_1)g(p_2) \rightarrow t(k_1)H^-(k_2)$  are shown in Fig.1. The amplitudes are created by use of Feynarts [8] and are handled with the help of FeynCalc [9]. As usual, we define the Mandelstam variables as

$$\begin{aligned} s &= (p_1 + p_2)^2 = (k_1 + k_2)^2, \\ t &= (p_1 - k_1)^2 = (p_2 - k_2)^2, \\ u &= (p_1 - k_2)^2 = (p_2 - k_1)^2. \end{aligned} \quad (2)$$

The amplitude of the tree-level diagrams could be written as

$$M_{Born} = \sum_{i=1}^6 t_i [c_1 M_{2i-1} + c_2 M_{2i}], \quad (3)$$

where the non-vanishing form factors are

$$\begin{aligned} t_2 &= \frac{1}{m_t^2(\mu) - u} - \frac{1}{s}, \\ t_3 &= \frac{2}{m_t^2(\mu) - u}, \\ t_5 &= -\frac{2}{s} \end{aligned} \quad (4)$$

with  $c_1 = \frac{g_w g m_b(\mu) \tan \beta}{2\sqrt{2}m_w}$  and  $c_2 = \frac{g_w g m_t(\mu) \cot \beta}{2\sqrt{2}m_w}$ . Here  $M_i$  is the standard matrix elements

$$M_1 = \bar{u}(k_1) \not{\epsilon}(p_2) P_R u(p_1),$$

$$M_2 = \bar{u}(k_1) \not{\epsilon}(p_2) P_L u(p_1),$$

$$\begin{aligned}
M_3 &= \bar{u}(k_1) \not{p}_2 \not{\epsilon}(k_2) P_R u(p_1), \\
M_4 &= \bar{u}(k_1) \not{p}_2 \not{\epsilon}(k_2) P_L u(p_1), \\
M_5 &= \bar{u}(k_1) P_R u(p_1) k_1 \cdot \epsilon(p_2), \\
M_6 &= \bar{u}(k_1) P_L u(p_1) k_1 \cdot \epsilon(p_2), \\
M_7 &= \bar{u}(k_1) \not{p}_2 P_R u(p_1) k_1 \cdot \epsilon(p_2), \\
M_8 &= \bar{u}(k_1) \not{p}_2 P_L u(p_1) k_1 \cdot \epsilon(p_2), \\
M_9 &= \bar{u}(k_1) P_R u(p_1) p_1 \cdot \epsilon(p_2), \\
M_{10} &= \bar{u}(k_1) P_L u(p_1) p_1 \cdot \epsilon(p_2), \\
M_{11} &= \bar{u}(k_1) \not{p}_2 P_R u(p_1) p_1 \cdot \epsilon(p_2), \\
M_{12} &= \bar{u}(k_1) \not{p}_2 P_L u(p_1) p_1 \cdot \epsilon(p_2),
\end{aligned} \tag{5}$$

where the color matrix  $T^a$  has been omitted.

The cross section can then be written as

$$\frac{d\sigma_{Born}}{dx_1 dx_2} = \frac{1}{24} \frac{1}{4} \frac{1}{2s} |M_{Born}|^2 d^N \Phi_2 G_{b/A}(x_1, \mu_f) G_{g/B}(x_2, \mu_f) + [A \leftrightarrow B], \tag{6}$$

where the factor  $\frac{1}{24}$  and  $\frac{1}{4}$  are the color and spin average, respectively, and two-body phase space is

$$d^N \Phi_2 = \frac{1}{8\pi} \left( \frac{4\pi}{s} \right)^\epsilon \frac{1}{\Gamma(1-\epsilon)} \left[ \lambda \left( 1, \frac{m_{H^\pm}^2}{s}, \frac{m_t^2}{s} \right) \right]^{1/2-\epsilon} v^{-\epsilon} (1-v)^{-\epsilon} dv, \tag{7}$$

with  $v = \frac{1}{2}(1 + \cos \theta)$ . In this paper, we perform the phase space integration in D-dimension with  $D = 4 - 2\epsilon$ . Here  $\lambda$  is the two-body phase space function

$$\lambda(x, y, z) = x^2 + y^2 + z^2 - 2xy - 2xz - 2yz. \tag{8}$$

## B. Virtual corrections

The diagrams from virtual corrections are shown in Fig. 2. The renormalized amplitude can be written in the following way,

$$M_{\text{ren}} = M_{\text{unren}} + M_{\text{con}}, \tag{9}$$

where  $M_{\text{unren}}$  and  $M_{\text{con}}$  are contributions from unrenormalization amplitude and conterterms.

The  $M_{\text{unren}}$  can be written as the sum of the virtual diagrams

$$M_{\text{unren}} = \sum_{i=e}^o M_{\text{unren}}^i, \quad (10)$$

where  $i$  represents the diagram index of Fig. 2. For each diagram  $i$ , we can generally write the amplitude as

$$M_{\text{unren}}^i = \sum_{j=1}^6 f_j [c_1 M_{2i-1} + c_2 M_{2i}], \quad (11)$$

where the non-vanishing form factor  $f_j$  are given explicitly in Appendix and the  $M_j$  is the standard matrix element given in the previous section.

In our calculations, we have used dimensional regularization to control the ultraviolet, infrared and collinear divergences. At the same time, the  $\overline{MS}$  renormalization and factorization schemes have been adopted. In the  $\overline{MS}$  renormalization scheme, the renormalization constants can be obtained by calculating the self-energy diagrams (a)-(d) in Fig. 2, which are given as

$$\begin{aligned} \frac{\delta m}{m} &\equiv \frac{\delta m_t}{m_t} = \frac{\delta m_b}{m_b} = -\frac{\alpha_s}{4\pi} 3C_F \Delta, \\ Z_q &\equiv Z_t = Z_b = -\frac{\alpha_s}{4\pi} C_F \Delta, \\ Z_g &= -\frac{\alpha_s}{4\pi} (2C_A - \beta_0) \Delta, \\ \frac{\delta g}{g} &= -\frac{\alpha_s}{8\pi} \beta_0 \Delta \end{aligned} \quad (12)$$

with  $\Delta = \frac{1}{\epsilon} - \gamma_E + \log(4\pi)$ ,  $\beta_0 = (11C_A - 2n_f)/3$ ,  $C_A = 3$  and  $C_F = 4/3$ . The  $M_{\text{con}}$  can be written as

$$M_{\text{con}} = \left( \frac{\delta g}{g} + \frac{\delta m}{m} + \frac{Z_g}{2} + 2Z_q \right) M_{\text{Born}} + M_{\text{Self}} + M_{\text{LSZ}}. \quad (13)$$

Here the  $M_{\text{Self}}$  and  $M_{\text{LSZ}}$  are the contributions from the diagrams with the conterterms on the internal quark lines and from the external quarks and gluon legs according to the LSZ prescription.  $M_{\text{Self}}$  can be written as

$$M_{\text{Self}} = \sum_{i=1}^6 f_s^i [c_1 M_{2i-1} + c_2 M_{2i}]. \quad (14)$$

The non-vanishing form factors  $f_s^i$  are

$$\begin{aligned}
f_s^1 &= \frac{m_t}{m_t^2 - u} \frac{\delta m}{m}, \\
f_s^2 &= \frac{-m_t^2(Z_q + 2\frac{\delta m}{m}) + uZ_q}{(m_t^2 - u)^2} + \frac{Z_q}{s}, \\
f_s^3 &= 2\frac{-m_t^2(Z_q + 2\frac{\delta m}{m}) + uZ_q}{(m_t^2 - u)^2}, \\
f_s^5 &= \frac{2Z_q}{s}.
\end{aligned} \tag{15}$$

The  $M_{LSZ}$  can be written as

$$M_{LSZ} = M_{Born} \frac{\alpha_s}{8\pi} \left[ -3\Delta + \frac{14}{3} \log(m_t^2/\mu^2) - \frac{4}{3}(4 + 6 \log 2) \right]. \tag{16}$$

After squaring the renormalized amplitude and performing the spin and color summations, the partonic cross section with virtual corrections can be written as

$$\frac{d\sigma^{Vir}}{dx_1 dx_2} = 2 \operatorname{Re} \overline{\sum} (M_{\text{ren}}^+ M_{Born}) d^N \Phi_2 G_{b/A}(x_1, \mu_f) G_{g/B}(x_2, \mu_f) + [A \leftrightarrow B]. \tag{17}$$

As usual,  $d\sigma^{Vir}$  contains infrared divergences after renormalization, which can only be cancelled by adding contributions from gluon-radiation. The remaining collinear divergences are absorbed by the redefinition of the parton distribution functions (PDF). In the next section, we will turn to the topic about real corrections.

### C. Real corrections

There are three kinds of real corrections for the processes  $bg \rightarrow tH^-$ : gluon-radiation [ $bg \rightarrow tH^-g$ ], initial-gluon [ $gg \rightarrow tH^-\bar{b}$ ] and initial light quarks [ $bq(\bar{q}) \rightarrow tH^-q(\bar{q})$  and  $q\bar{q} \rightarrow tH^-\bar{b}$ ,  $q$  is the light quarks  $u, d$  and  $s$ ]. All real corrections are related to the  $2 \rightarrow 3$  processes. In this paper, the real corrections have been computed using the two cut-off phase space slicing method (TCPSSM) [10]. The main idea of TCPSSM is to introduce two small constants  $\delta_s, \delta_c$ . The three-body phase space can then be divided into soft and hard regions according to parameter  $\delta_s$ , and the hard region is further divided into collinear and non-collinear regions according to parameter  $\delta_c$ . In the soft and collinear regions, approximations can be made and analytical results can be easily obtained. In the non-collinear region, numerical results can be calculated in four dimension by standard Monte Carlo packages because it contains no divergences. The physical results should be independent on these

artificial parameters  $\delta_s$  and  $\delta_c$ , which offers a crucial way to check our results. Therefore, the real corrections can be written as, according to the phase space slicing,

$$d\sigma^{Real} = d\sigma_S + d\sigma_{Coll} + d\sigma_{finite}. \quad (18)$$

### 1. Contributions in soft region

In soft region, only the gluon-radiation process  $bg \rightarrow tH^-g$ , the Feynman diagrams of the process are shown in Fig. 3, is relevant. We may write the contributions in soft region as

$$\frac{d\sigma_S}{dx_1 dx_2} = d\hat{\sigma}^0 \left[ \frac{\alpha_s}{2\pi} \frac{\Gamma(1-\epsilon)}{\Gamma(1-2\epsilon)} \left( \frac{4\pi\mu_r^2}{s} \right)^\epsilon \right] \left( \frac{A_2^s}{\epsilon^2} + \frac{A_1^s}{\epsilon} + A_0^s \right) G_{b/A}(x_1, \mu_f) G_{g/B}(x_2, \mu_f) + [A \leftrightarrow B], \quad (19)$$

where

$$\begin{aligned} A_2^s &= -\frac{4}{3} \frac{m_t^2 - t}{(E_1 - \beta \cos \theta)_s} + 12 \frac{m_t^2 - u}{(E_1 + \beta \cos \theta)_s} + 12, \\ A_1^s &= \frac{16}{3} \frac{4m_t^2}{(E_1^2 - \beta^2)_s} + \frac{4}{3} \frac{m_t^2 - t}{(E_1 - \beta \cos \theta)_s} (C_1 - 2 \log \frac{2}{\delta_s \sqrt{s}}) \\ &\quad + 12 \frac{m_t^2 - u}{(E_1 + \beta \cos \theta)_s} (C_2 - 2 \log \frac{2}{\delta_s \sqrt{s}}) + 24 \log \frac{2}{\delta_s \sqrt{s}} - \log \frac{4}{s} A_2^s, \\ A_0^s &= \frac{1}{2} \log^2 \frac{4}{s} A_2^s - \log \frac{4}{s} A_1^s + \frac{16}{3} \frac{4m_t^2}{(E_1^2 - \beta^2)_s} (2 \log \frac{2}{\delta_s \sqrt{s}} + \frac{E_1}{\beta} \log \frac{E_1 + \beta}{E_1 - \beta}) \\ &\quad + \frac{4}{3} \frac{m_t^2 - t}{(E_1 - \beta \cos \theta)_s} (C_3 - 2 \log^2 \frac{2}{\delta_s \sqrt{s}} + 2C_1 \log \frac{2}{\delta_s \sqrt{s}}) \\ &\quad - 12 \frac{m_t^2 - u}{(E_1 + \beta \cos \theta)_s} (C_4 - 2 \log^2 \frac{2}{\delta_s \sqrt{s}} + 2C_2 \log \frac{2}{\delta_s \sqrt{s}}) + 24 \log^2 \frac{2}{\delta_s \sqrt{s}}, \\ C_1 &= \log \frac{(E_1 - \beta \cos \theta)^2}{E_1^2 - \beta^2}, \\ C_2 &= \log \frac{(E_1 + \beta \cos \theta)^2}{E_1^2 - \beta^2}, \\ C_3 &= -\log^2 \frac{E_1 - \beta}{E_1 - \beta \cos \theta} + \frac{1}{2} \log^2 \frac{E_1 + \beta}{E_1 - \beta} - 2li_2\left(-\frac{-\beta \cos \theta + \beta}{E_1 - \beta}\right) + 2li_2\left(-\frac{\beta \cos \theta + \beta}{E_1 - \beta \cos \theta}\right), \\ C_4 &= -\log^2 \frac{E_1 - \beta}{E_1 + \beta \cos \theta} + \frac{1}{2} \log^2 \frac{E_1 + \beta}{E_1 - \beta} - 2li_2\left(-\frac{\beta \cos \theta + \beta}{E_1 - \beta}\right) + 2li_2\left(-\frac{-\beta \cos \theta + \beta}{E_1 + \beta \cos \theta}\right), \\ \beta &= \lambda^{\frac{1}{2}}(1, m_t^2/s, m_{H^\pm}^2/s), \\ E_1 &= \sqrt{\beta^2 + \frac{2m_t^2}{s}}. \end{aligned} \quad (20)$$

## 2. Contributions in collinear region

In order to absorb the collinear singularity, we should introduce a scale dependent parton distribution function. Using the  $\overline{\text{MS}}$  convention and after factorization, we can write:

$$\begin{aligned} \frac{d\sigma_{Coll}}{dx_1 dx_2} = & \left[ \frac{\alpha_s}{2\pi} \frac{\Gamma(1-\epsilon)}{\Gamma(1-2\epsilon)} \left( \frac{4\pi\mu_r^2}{s} \right)^\epsilon \right] \left\{ G_{b/A}(x_1, \mu_f) G_{g/B}(x_2, \mu_f) \right. \\ & \times \left[ \frac{A_1^{sc}(b \rightarrow bg)}{\epsilon} + \frac{A_1^{sc}(g \rightarrow gg)}{\epsilon} + A_0^{sc}(b \rightarrow bg) + A_0^{sc}(g \rightarrow gg) \right] \\ & + G_{b/A}(x_1, \mu_f) \tilde{G}_{g/B}(x_2, \mu_f) + \tilde{G}_{b/A}(x_1, \mu_f) G_{g/B}(x_2, \mu_f) \left. \right\} d\hat{\sigma}_0^{Born} \\ & + [A \leftrightarrow B], \end{aligned} \quad (21)$$

where [10]

$$A_0^{sc} = A_1^{sc} \ln \left( \frac{s}{u_f^2} \right) \quad (22)$$

$$A_1^{sc}(b \rightarrow bg) = C_F(2 \ln \delta_s + 3/2) \quad (23)$$

$$A_1^{sc}(g \rightarrow gg) = 2N \ln \delta_s + (11N - 2n_f)/6. \quad (24)$$

Here

$$\tilde{G}_{c/B,A}(x, \mu_f) = \sum_{c'} \int_x^{1-\delta_s \delta_{cc'}} \frac{dy}{y} G_{c'/B,A}(x/y, \mu_f) \tilde{P}_{cc'}(y) \quad (25)$$

with

$$\tilde{P}_{ij}(y) = P_{ij}(y) \ln \left( \delta_c \frac{1-y}{y} \frac{s}{\mu_f^2} \right) - P'_{ij}(y), \quad (26)$$

where

$$P_{qq}(z) = C_F \frac{1+z^2}{1-z} \quad (27)$$

$$P'_{qq}(z) = -C_F(1-z) \quad (28)$$

$$P_{gq}(z) = C_F \frac{1+(1-z)^2}{z} \quad (29)$$

$$P'_{gq}(z) = -C_F z \quad (30)$$

$$P_{gg}(z) = 2N \left[ \frac{z}{1-z} + \frac{1-z}{z} + z(1-z) \right] \quad (31)$$

$$P'_{gg}(z) = 0 \quad (32)$$

$$P_{qq}(z) = \frac{1}{2} [z^2 + (1-z)^2] \quad (33)$$

$$P'_{qq}(z) = -z(1-z), \quad (34)$$

with  $N = 3$ .



### 3. Contributions in non-collinear region

As described above, the contributions in non-collinear region can be easily obtained by Monte Carlo integration in four dimension. The  $d\sigma_{finite}$  can be written as

$$\frac{d\sigma_{finite}}{dx_1 dx_2} = \sum_{q,q'} G_{q/A}(x_1, \mu_f) G_{q'/B}(x_2, \mu_f) |(qq' \rightarrow tH^- X)|^2 d\Phi_3 + [A \leftrightarrow B], \quad (35)$$

where  $q, q'$  run through gluon and quarks and the three-body phase space  $\Phi_3$  is within the non-collinear region. In this paper, all Monte Carlo integrations are performed by package BASES [11].

## III. NUMERICAL RESULTS AND DISCUSSION

Our numerical results are obtained using CTEQ5M (CTEQ5L) PDF [12] for NLO (LO) cross-section calculations. The 2-loop evolution of  $\alpha_s(\mu)$  and  $\overline{MS}$  quark masses is adopted and  $\alpha_s(M_Z) = 0.118$ . The top-quark pole mass is taken to be  $m_t = 175$  GeV; for simplicity, the bottom-quark mass has been omitted, and the renormalization and factorization scales are taken to be the same.

In Fig. 4 we show the K-factors, which are defined as

$$K = \frac{\sigma_{NLO}}{\sigma_{LO}}, \quad (36)$$

as a function of the charged Higgs mass, where the renormalization and factorization scales  $\mu = \mu_0$  ( $\mu_0 = m_t + m_W$ ). Here the  $\sigma_{NLO}$  can be the contributions arising from Born, virtual+gluon-radiation, initial-gluon,  $bq(\bar{q})$  ( $q$  is the light quark  $u, d$  and  $s$ ) and  $q\bar{q}$ . It should be noted here that the QCD corrections do not depend on the  $\tan\beta$ , because the QCD interaction does not change the chiral structure of the considered processes. From the figure, we can see that K-factor of Born contribution, which are due to the difference between the LO and NLO PDF, is around 1.2. K-factor of virtual+gluon-radiation contributions is from 0.6 to 0.85 when the charged Higgs boson mass varies from 180 GeV to 1000 GeV. The initial-gluon and  $bq(\bar{q})$  contribution are negative, and vary from  $\sim -27\%$  to  $\sim -22\%$  as well as  $\sim -13\%$  to  $\sim -5\%$  respectively. The  $q\bar{q}$  contribution can be neglected, which is smaller than 3% for all charged Higgs boson mass. Adding all the contributions, the total

K-factor varies from  $\sim 1.55$  to  $\sim 1.75$  when charged Higgs mass increases from 180 GeV to 1000 GeV.

In Fig. 5 we show the tree level and NLO cross sections as a function of renormalization and factorization scales  $\mu/\mu_0$  for several charged Higgs mass samples and  $\tan\beta = 50$ . From the figure we can see that the NLO result is greater than the lowest order one. Moreover the NLO QCD corrections reduce the scales dependence compared to that at tree level.

To summarize, the next-to-leading order QCD corrections to charged Higgs boson associated production with top quark through  $bg \rightarrow tH^-$  at the CERN Large Hadron Collider are calculated in the minimal supersymmetric standard model and two-Higgs-doublet model in the  $\overline{MS}$  scheme. The NLO QCD corrections can reduce the scales dependence compared to that at tree level, and the K-factor varies from  $\sim 1.55$  to  $\sim 1.75$  when charged Higgs mass increases from 180 GeV to 1000 GeV. We should note here that the results presented in this paper are for the process  $bg \rightarrow tH^-$ ; they are the same for the charge conjugate process  $\bar{b}g \rightarrow H^+\bar{t}$ . Moreover, because the QCD corrections do not change the chiral structure of the processes, our results are also valid for other models, which contain the  $t - \bar{b} - H^-$  ( $\bar{t} - b - H^+$ ) interactions.

#### IV. ACKNOWLEDGEMENT

The author would like to thank Prof. W. Hollik and Prof. C.S. Li for stimulating discussions. This work was supported in part by the Alexander von Humboldt Foundation and National Nature Science Foundation of China. Parts of the calculations have been performed on the QCM cluster at the University of Karlsruhe, supported by the DFG-Forschergruppe "Quantenfeldtheorie, Computeralgebra und Monte-Carlo-Simulation".

- 
- [1] For example to see, L. G. Jin, C. S. Li, R. J. Oakes and S. H. Zhu, Phys. Rev. D **62**, 053008 (2000) [arXiv:hep-ph/0003159], and references therein.
- [2] W. Hollik and S. H. Zhu, hep-ph/0109103.
- [3] D. P. Roy, Phys. Lett. B **459**, 607 (1999) [arXiv:hep-ph/9905542].
- [4] K. Odagiri, Phys. Lett. B **452**, 327 (1999) [arXiv:hep-ph/9902303].
- [5] F. Borzumati, J. L. Kneur and N. Polonsky, Phys. Rev. D **60**, 115011 (1999) [arXiv:hep-ph/9905443].
- [6] L. G. Jin, C. S. Li, R. J. Oakes and S. H. Zhu, Eur. Phys. J. C **14**, 91 (2000) [arXiv:hep-ph/9907482].
- [7] A. Belyaev, D. Garcia, J. Guasch and J. Sola, arXiv:hep-ph/0105053; C. S. Huang and S. H. Zhu, Phys. Rev. D **60**, 075012 (1999) [arXiv:hep-ph/9812201].
- [8] J. Küblbeck, M. Böhm and A. Denner, Comput. Phys. Commun. **60**, 165 (1990); T. Hahn, hep-ph/9905354.
- [9] R. Mertig, M. Böhm and A. Denner, Comput. Phys. Commun. **64**, 345 (1991).
- [10] For example to see, B. W. Harris and J. F. Owens, hep-ph/0102128; S. H. Zhu, arXiv:hep-ph/0109269, to appear in Phys. Lett. B.
- [11] S. Kawabata, Comput. Phys. Commun. **88**, 309 (1995).
- [12] H. L. Lai *et al.* [CTEQ Collaboration], Eur. Phys. J. C **12**, 375 (2000) [hep-ph/9903282].
- [13] G. J. van Oldenborgh and J. A. Vermaseren, Z. Phys. C **46**, 425 (1990).

## V. APPENDIX

In this appendix, we will give the non-vanishing form-factors in Eq. (11). For simplicity, we define abbreviation for  $B_0^i (i = 1 - 7)$ ,  $C_x^i (i = 1 - 8)$ ,  $D_0^i (i = 1 - 3)$  as

$$\begin{aligned}
B_0^1 &= B_0(0, 0, m_t^2), \\
B_0^2 &= B_0(0, m_t^2, m_t^2), \\
B_0^3 &= B_0(m_{H^\pm}^2, 0, m_t^2), \\
B_0^4 &= B_0(m_t^2, 0, m_t^2), \\
B_0^5 &= B_0(s, 0, 0), \\
B_0^6 &= B_0(t, 0, m_t^2), \\
B_0^7 &= B_0(u, 0, m_t^2), \\
C_x^1 &= C_x(0, 0, s, 0, 0, 0), \\
C_x^2 &= C_x(0, m_{H^\pm}^2, t, m_t^2, m_t^2, 0), \\
C_x^3 &= C_x(m_{H^\pm}^2, 0, t, m_t^2, 0, 0), \\
C_x^4 &= C_x(m_{H^\pm}^2, 0, u, m_t^2, 0, 0), \\
C_x^5 &= C_x(m_{H^\pm}^2, m_t^2, s, 0, m_t^2, 0), \\
C_x^6 &= C_x(m_t^2, 0, t, m_t^2, 0, 0), \\
C_x^7 &= C_x(m_t^2, 0, u, 0, m_t^2, m_t^2), \\
C_x^8 &= C_x(m_t^2, 0, u, m_t^2, 0, 0), \\
D_0^1 &= D_0(m_{H^\pm}^2, 0, m_t^2, 0, t, u, 0, m_t^2, m_t^2, 0), \\
D_0^2 &= D_0(m_{H^\pm}^2, m_t^2, 0, 0, s, t, 0, m_t^2, 0, 0), \\
D_0^3 &= D_0(m_{H^\pm}^2, m_t^2, 0, 0, s, u, 0, m_t^2, 0, 0).
\end{aligned} \tag{37}$$

For diagram (e) in Fig. 2, we can write the form factor as

$$f_i = \frac{C_A}{2} \frac{g_s^3}{16\pi^2 s} g_i \tag{38}$$

$$\begin{aligned}
g_2 &= -2B_0^5 - s[C_0^1 + 3(C_1^1 + C_2^1)] + 4(-1 + 2\epsilon)C_{00}^1, \\
g_5 &= 2[B_0^5(1 + \epsilon) + s(C_0^1 + 2C_1^1 - 3C_2^1)].
\end{aligned} \tag{39}$$

For diagram (f) in Fig. 2, we can write the form factor as

$$f_i = (C_F - C_A/2) \frac{g_s^3}{8\pi^2 s} g_i \quad (40)$$

$$\begin{aligned} g_2 &= -B_0^5 - (1 + \epsilon)s(C_0^1 + C_1^1 + C_2^1) + 2(1 - \epsilon)C_{00}^1, \\ g_5 &= (1 + \epsilon)B_0^5 + 2\epsilon s C_1^1 - 2(1 + \epsilon)s C_2^1. \end{aligned} \quad (41)$$

For diagram (g) in Fig. 2, we can write the form factor as

$$f_i = C_F \frac{g_s^3}{8\pi^2 s} g_i \quad (42)$$

$$\begin{aligned} g_1 &= m_t s (C_0^5 (1 - \epsilon) + C_2^5 - \epsilon(C_1^5 + C_2^5)), \\ g_2 &= \frac{g_5}{2} = C_0^5 (m_{H^\pm}^2 - 2m_t^2) - B_0^4 - B_0^5 - m_t^2 (C_1^5 + C_2^5) + \epsilon(B_0^3 + s C_2^5). \end{aligned} \quad (43)$$

For diagram (h) in Fig. 2, we can write the form factor as

$$f_i = C_F \frac{g_s^3}{8\pi^2 (m_t^2 - u)} g_i \quad (44)$$

$$\begin{aligned} g_1 &= m_t (-1 + \epsilon) (m_t^2 - u) (C_0^4 + C_1^4 + C_2^4), \\ g_2 &= \frac{g_3}{2} = -C_0^4 [m_{H^\pm}^2 + (-2 + \epsilon)m_t^2 - \epsilon u] + B_0^7 \\ &\quad + m_t^2 (C_1^4 + C_2^4) - \epsilon [B_0^3 + (m_t^2 - u) (C_1^4 + C_2^4)]. \end{aligned} \quad (45)$$

For diagram (i) in Fig. 2, we can write the form factor as

$$f_i = \frac{C_A}{2} \frac{g_s^3}{16\pi^2 (m_t^2 - u)} g_i \quad (46)$$

$$\begin{aligned} g_1 &= 3m_t (m_t^2 - u) C_2^8, \\ g_2 &= 2B_0^4 + 2B_0^7 + (m_t^2 - u) (2C_0^8 + 3C_1^8) + 4(1 - \epsilon) C_{00}^8, \\ g_3 &= 2\{\epsilon - 1 + C_0^8 (m_t^2 - u) - (1 + \epsilon) B_0^4 + 2B_0^7 + m_t^2 [-5C_1^8 + 4C_2^8 + 2(1 - \epsilon) C_{11}^8] \\ &\quad + u [C_1^8 - 4C_2^8 - 2(1 - \epsilon) C_{11}^8]\}, \\ g_4 &= 4m_t [C_1^8 - 2C_2^8 - (1 - \epsilon) C_{11}^8]. \end{aligned} \quad (47)$$

For diagram (j) in Fig. 2, we can write the form factor as

$$f_i = (C_F - C_A/2) \frac{g_s^3}{8\pi^2(m_t^2 - u)} g_i \quad (48)$$

$$\begin{aligned} g_1 &= m_t(m_t^2 - u)[C_2^7 + \epsilon(C_0^7 + C_2^7)], \\ g_2 &= 2C_0^7 m_t^2 - (1 + \epsilon)B_0^2 + B_0^4 + B_0^7 + (1 + \epsilon)(m_t^2 - u)C_1^7 + 2(-1 + \epsilon)C_{00}^7, \\ g_3 &= -1 - B_0^4 + 2B_0^7 + 2uC_{22}^7 - 2m_t^2(2C_2^7 + C_{22}^7) \\ &\quad - \epsilon[-1 + B_0^4 - 2(m_t^2 - u)(C_2^7 + C_{22}^7)], \\ g_4 &= -2m_t[C_0^7 \epsilon + (-1 + 2\epsilon)C_2^7 + (-1 + \epsilon)C_{22}^7]. \end{aligned} \quad (49)$$

For diagram (k) in Fig. 2, we can write the form factor as

$$f_i = C_F \frac{g_s^3}{16\pi^2 s} g_i \quad (50)$$

$$g_2 = \frac{g_5}{2} = (1 - \epsilon)B_0^5. \quad (51)$$

For diagram (l) in Fig. 2, we can write the form factor as

$$f_i = C_F \frac{g_s^3}{16\pi^2(m_t^2 - u)^2 u} g_i \quad (52)$$

$$\begin{aligned} g_1 &= -m_t(m_t^2 - u) \left\{ (\epsilon - 1)m_t^2(B_0^1 - B_0^7) + u(\epsilon - 3)B_0^7 \right\}, \\ g_2 &= \frac{g_3}{2} = (-1 + \epsilon)m_t^4(B_0^1 - B_0^7) - (-1 + \epsilon)u^2 B_0^7 \\ &\quad + m_t^2 u \left\{ (1 - \epsilon)[B_0^1 - 2(1 + B_0^2)] + 2(-3 + \epsilon)B_0^7 \right\}. \end{aligned} \quad (53)$$

For diagram (m) in Fig. 2, we can write the form factor as

$$f_i = \frac{C_A}{2} \frac{g_s^3}{16\pi^2} g_i \quad (54)$$

$$\begin{aligned} g_1 &= -m_t[C_0^8 + C_1^8 + C_2^8 - 2(s - u + m_t^2)(D_0^3 + D_1 + D_2 + D_3) + 4D_{00}], \\ g_2 &= -2(C_0^4 + C_0^5) - 2D_0^3(m_t^2 - u) + C_1^1 + C_1^8 + 2(t + 2u)(D_2 + D_3) \\ &\quad - m_{H^\pm}^2(D_1 + 2D_2 + D_3) - m_t^2(D_1 + 4D_2 + 3D_3) + 4\epsilon D_{00}, \\ g_3 &= -2 \left\{ 2[C_0^4 - (1 + \epsilon)C_0^5 + C_0^8] - 2\epsilon(C_1^5 + C_2^5) + C_1^8 + C_2^8 + 2D_0^3[-m_{H^\pm}^2 + (1 - \epsilon)m_t^2 \right. \\ &\quad \left. + (1 + \epsilon)u] + 2[(3 - 2\epsilon)m_t^2 - t + 2u\epsilon](D_1 + D_2 + D_3) + 2[(1 - \epsilon)m_t^2 + u\epsilon](D_{11} \right. \end{aligned}$$

$$\begin{aligned}
& +2D_{12} + 2D_{13} + D_{22} + 2D_{23} + D_{33})\}, \\
g_4 = & 4m_t \left\{ (D_2 + D_3 + D_{11} + 2D_{12} + D_{13} + D_{22} + D_{23}) - \epsilon[D_0^3 + D_{11} + D_{22} + D_{33} \right. \\
& \left. + 2(D_1 + D_2 + D_3 + D_{12} + D_{13} + D_{23})] \right\}, \\
g_5 = & 4m_t \left\{ C_0^1 + 2\epsilon C_1^5 - C_1^1 + 2(u - m_t^2)D_1 + [m_{H^\pm}^2 - (7 - 2\epsilon)m_t^2 + 2(t + 2u) - 2u\epsilon]D_2 \right. \\
& \left. + [-m_{H^\pm}^2 - m_t^2 + 2s]D_3 + [2(\epsilon - 1)m_t^2 - 2u\epsilon](D_{12} + D_{22} + D_{23}) \right\}, \\
g_6 = & -4m_t[D_0^3 + D_1 + (2 - \epsilon)D_2 + D_3 + D_{12} + D_{22}], \tag{55}
\end{aligned}$$

where the variable of the D-function is the same with  $D_0^3$ .

For diagram (n) in Fig. 2, we can write the form factor as

$$f_i = (C_F - C_A/2) \frac{g_s^3}{8\pi^2} g_i \tag{56}$$

$$\begin{aligned}
g_1 = & -m_t \left\{ D_0^1[s + \epsilon(m_t^2 - u)] + s(D_2 + D_3) \right. \\
& \left. - \epsilon[C_2^6 - m_t^2(D_1 + D_3) + u(D_2 + D_3)] - 2D_{00} \right\}, \\
g_2 = & -C_0^4 - C_0^7 + C_0^2(2 + \epsilon) + D_0^1[m_{H^\pm}^2 + \epsilon m_t^2 - (2 + \epsilon)u] + D_1[m_t^2(1 + \epsilon) \\
& + s - u(1 + \epsilon)] + (D_2 + D_3)[\epsilon m_t^2 + s - u(1 + \epsilon)] - 2\epsilon D_{00}, \\
g_3 = & 2 \left\{ -C_0^4 - C_0^7 - (C_1^7 + C_2^7) - \epsilon(C_1^2 + C_2^6) + 2m_t^2 D_2 - t(D_2 + D_3) + m_t^2(2D_3 + D_{22} \right. \\
& \left. + 2D_{23} + D_{33}) - \epsilon[C_2 + (m_t^2 - u)(D_2 + D_3 + D_{22} + 2D_{23} + D_{33})] \right\}, \\
g_4 = & 2m_t \left\{ -D_2 - D_3 - D_{12} - D_{13} - D_{22} - 2D_{23} - D_{33} \right. \\
& \left. + \epsilon[D_0^1 + 2D_2 + 2D_3 + D_{22} + 2D_{23} + D_{33}] \right\}, \\
g_5 = & -2 \left\{ C_0^6(-1 + \epsilon) + (4m_t^2 - t - 2u)D_2 - sD_3 + m_t^2(D_{22} + D_{23}) \right. \\
& \left. + \epsilon[2C_1^6 - C_1^2 + C_2^6 - (m_t^2 - u)(D_3 + D_{22} + D_{23})] \right\}, \\
g_6 = & 2m_t[D_0 - (-3 + \epsilon)D_2 + D_{12} - (-1 + \epsilon)(D_{22} + D_{23})], \tag{57}
\end{aligned}$$

where the variable of the D-function is the same with  $D_0^1$ .

For diagram (o) in Fig. 2, we can write the form factor as

$$f_i = (C_F - C_A/2) \frac{g_s^3}{8\pi^2} g_i \tag{58}$$

$$\begin{aligned}
g_1 = & -m_t[C_0^5 - \epsilon C_0^6 + D_0^2(1 + \epsilon)s - \epsilon(C_1^6 + C_2^6) + s(1 + \epsilon)(D_1 + D_2 + D_3) - 2D_{00}], \\
g_2 = & -C_0^1 - C_0^5 + C_0^3(2 + \epsilon) + D_0^2(-2m_t^2 + t) - m_t^2(D_1 + D_2)
\end{aligned}$$

$$\begin{aligned}
& +[s(1+\epsilon) - u]D_3 - 2\epsilon D_{00}, \\
g_3 = & 2 \left\{ C_0^5(1+\epsilon) - C_0^6\epsilon + D_0^2[2m_{H^\pm}^2 + m_t^2(4-\epsilon) - s(2-\epsilon) - 3t - u(2-\epsilon)] \right. \\
& + \epsilon(C_1^3 + C_1^5 - C_1^6 + C_2^5 - C_2^6) + (D_1 + D_2 + D_3)[m_{H^\pm}^2(-3+\epsilon) - m_t^2\epsilon + 3s + t(2-\epsilon) \\
& \left. + u(3+\epsilon)] + (D_{11} + 2D_{12} + 2D_{13} + D_{22} + 2D_{23} + D_{33})[m_t^2(1-\epsilon) + \epsilon u] \right\}, \\
g_4 = & 2m_t \left\{ -D_3 - D_{13} - D_{23} - D_{33} + \epsilon(D_0 + 2D_1 + 2D_2 + 2D_3 + D_{11} \right. \\
& \left. + 2D_{12} + 2D_{13} + D_{22} + 2D_{23} + D_{33}) \right\}, \\
g_5 = & -2 \left\{ C_0^6 - D_0^2(m_{H^\pm}^2 - 2m_t^2) - C_1^1 + \epsilon(C_1^3 + C_2^5) + D_1[-t(1+\epsilon) - 2u] + \right. \\
& (D_2 + D_3)[\epsilon m_{H^\pm}^2 - s(1+\epsilon)] + D_3[-t(1+\epsilon) - u] + (D_{11} + D_{12} + 2D_{13} + D_{23} + D_{33})u\epsilon \\
& \left. + m_t^2[5D_1 + D_2 + 4D_3 - (-1+\epsilon)(D_{11} + D_{12} + 2D_{13} + D_{23} + D_{33})] \right\}, \\
g_6 = & 2m_t \left\{ D_0^2 - (-2+\epsilon)(D_1 + D_3) + D_{13} + D_{33} - \epsilon(D_{11} + D_{12} + 2D_{13} + D_{23} + D_{33}) \right\}, \quad (59)
\end{aligned}$$

where the variable of the D-function is the same with  $D_0^2$ .

Through decomposition, the loop integrations in above form-factors can be calculated by the limit number of scalar integrates  $B_0, C_0$  and  $D_0$ . Some of the scalar integrates  $C_0$  and  $D_0$  contain infrared and collinear divergences. Because the finit scalars integration could be calculated by numerical method [13], we present here only the divergent scalars integrations.

$D_0$  and  $C_0$  scalar integrates could be written as

$$\begin{aligned}
D_0 &= \frac{(4\pi\mu^2)^\epsilon \Gamma(2+\epsilon)}{1+\epsilon} \left( \frac{d_2}{\epsilon^2} + \frac{d_1}{\epsilon} + d_0 \right), \\
C_0 &= -(4\pi\mu^2)^\epsilon \Gamma(1+\epsilon) \left( \frac{c_2}{\epsilon^2} + \frac{c_1}{\epsilon} + c_0 \right). \quad (60)
\end{aligned}$$

The coefficients of  $D_0^1$  are

$$d_2 = \frac{1}{2(-t + m_t^2)(-u + m_t^2)}, \quad (61)$$

$$d_1 = \frac{\log(m_t) - \log(-t + m_t^2) - \log(-u + m_t^2) + \log(-m_{H^\pm}^2 + m_t^2)}{(-t + m_t^2)(-u + m_t^2)}, \quad (62)$$

$$\begin{aligned}
d_0 = & \frac{1}{2(-t + m_t^2)(-u + m_t^2)} \left\{ 6\log^2(m_t) + 8\log(m_{H^\pm})\log(m_t) - 4\log(m_t^2 - t)\log(m_t) \right. \\
& - 4\log(t)\log(m_t) - 4\log(m_t^2 - t)\log(m_t) - 4\log(u)\log(m_t) + 4\log|m_{H^\pm}^2 - m_t^2|\log(m_t) \\
& \left. + \log^2(m_t^2 - t) + \log^2(m_t^2 - u) - \log^2|m_{H^\pm}^2 - m_t^2| - 4\log^2(m_t^2 - t)\log^2(m_{H^\pm}^2 - t) \right\}
\end{aligned}$$



$$\begin{aligned}
& +2\log^2(m_t^2 - t)\log(t) + 8\log(m_t^2 - t)\log(m_t^2 - u) - 4\log^2(m_t^2 - u)\log^2(m_{H^\pm}^2 - u) \\
& +2\log^2(m_t^2 - u)\log(u) - 4\log(m_{H^\pm})\log|m_{H^\pm}^2 - m_t^2| + 4\log(m_{H^\pm}^2 - t)\log|m_{H^\pm}^2 - m_t^2| \\
& -4\log(m_t^2 - t)\log|m_{H^\pm}^2 - m_t^2| + 4\log(m_{H^\pm}^2 - u)\log|m_{H^\pm}^2 - m_t^2| \\
& -4\log(m_t^2 - u)\log|m_{H^\pm}^2 - m_t^2| + 2li_2\left(\frac{tu - m_{H^\pm}^2 m_t^2}{(m_{H^\pm}^2 - t)(m_{H^\pm}^2 - u)}\right) + 2li_2\left(\frac{m_{H^\pm}^2 m_t^2 - tu}{m_t^2(m_{H^\pm}^2 - u)}\right) \\
& +2li_2\left(\frac{m_{H^\pm}^2}{m_{H^\pm}^2 - m_t^2}\right) - 2li_2\left(\frac{s}{-t + m_t^2}\right) - 2li_2\left(\frac{t}{t - m_t^2}\right) - 2li_2\left(\frac{m_{H^\pm}^2 - t}{m_t^2 - u} + 1\right) \\
& +2li_2\left(\frac{(m_{H^\pm}^2 - m_t^2)s}{(m_t^2 - t)(u - m_t^2)}\right) - 2li_2\left(\frac{u}{u - m_t^2}\right) + 2li_2\left(\frac{m_{H^\pm}^2 m_t^2 - tu}{m_t^2(m_{H^\pm}^2 - t)}\right) \\
& -2li_2\left(\frac{(m_{H^\pm}^2 - m_t^2)(m_{H^\pm}^2 m_t^2 - tu)}{m_t^2(m_{H^\pm}^2 - u)(m_{H^\pm}^2 - t)}\right) - 2li_2\left(\frac{m_{H^\pm}^2 m_t^2 - tu}{(m_{H^\pm}^2 - t)(m_t^2 - t)}\right) \\
& +2li_2\left(\frac{tu - m_{H^\pm}^2 m_t^2}{(m_t^2 - t)(m_t^2 - u)}\right) - 2li_2\left(\frac{m_{H^\pm}^2 m_t^2 - tu}{(m_{H^\pm}^2 - u)(m_t^2 - u)}\right) + \pi^2\theta(m_{H^\pm} - m_t) \Big\}. \quad (63)
\end{aligned}$$

The coefficients of  $D_0^2$  are

$$d_2 = -\frac{3}{2s(-t + m_t^2)}, \quad (64)$$

$$d_1 = \frac{1}{s(-t + m_t^2)} \left\{ 4\log(m_t^2 - t) - \log(m_{H^\pm}^2 - t) + 2\log(s) - \log(m_t^2) - \log(m_{H^\pm}^2 - m_t^2) \right\}, \quad (65)$$

$$\begin{aligned}
d_0 = \frac{1}{2s(-t + m_t^2)} \Big\{ & \pi^2 \left[ \frac{4}{3} - \theta(m_{H^\pm} - m_t) \right] + 2\log^2(m_t) + 4\log(m_t) [\log(s) + \log(m_{H^\pm}^2 - t) \\
& - 2\log|m_{H^\pm}^2 - m_t^2|] + 3\log^2|m_{H^\pm}^2 - m_t^2| - \log(m_t^2 - t) [4\log(s) - 2\log(m_{H^\pm}^2 - t) \\
& + 3\log(m_t^2 - t)] + 4\log|m_{H^\pm}^2 - m_t^2| [\log(m_t^2 - t) - \log(m_{H^\pm}^2 - t)] + 2li_2\left(\frac{m_t^2}{m_t^2 - m_{H^\pm}^2}\right) \\
& - 2li_2\left(\frac{t}{m_t^2}\right) + 2li_2\left(\frac{(m_{H^\pm}^2 - m_t^2)t}{m_t^2(m_{H^\pm}^2 - t)}\right) - 2li_2\left(\frac{t}{t - m_{H^\pm}^2}\right) - 2li_2\left(\frac{m_{H^\pm}^2 - m_t^2}{t - m_t^2}\right) \Big\}. \quad (66)
\end{aligned}$$

The coefficients of  $C_0^1$  are

$$c_2 = -\frac{1}{s}, \quad (67)$$

$$c_1 = \frac{\log(s)}{s}, \quad (68)$$

$$c_0 = \frac{1}{6s} [4\pi^2 - 3\log^2(s)]. \quad (69)$$

The coefficients of  $C_0^3$  are

$$c_1 = \frac{1}{m_{H^\pm}^2 - t} \log \left( \frac{m_t^2 - m_{H^\pm}^2}{m_t^2 - t} \right), \quad (70)$$

$$c_0 = \frac{1}{m_{H^\pm}^2 - t} \left\{ -\frac{1}{2} \log^2 |m_{H^\pm}^2 - m_t^2| + \frac{1}{2} \log^2(m_t^2 - t) + \log \left( 1 - \frac{m_{H^\pm}^2}{m_t^2} \right) \log \left( \frac{m_{H^\pm}^2}{m_{H^\pm}^2 - m_t^2} \right) \right. \\ \left. - \log \left( \frac{t}{t - m_t^2} \right) \log \left( 1 - \frac{t}{m_t^2} \right) - li_2 \left( \frac{m_t^2}{m_t^2 - m_{H^\pm}^2} \right) + li_2 \left( \frac{m_t^2}{m_t^2 - t} \right) \right\}. \quad (71)$$

The coefficients of  $C_0^6$  are

$$c_2 = \frac{1}{2(m_t^2 - t)}, \quad (72)$$

$$c_1 = \frac{1}{2(m_t^2 - t)} \left\{ \log(m_t^2) - 2 \log(m_t^2 - t) \right\}, \quad (73)$$

$$c_0 = \frac{1}{4(m_t^2 - t)} \left\{ -\frac{2}{3} \pi^2 - \log(m_t^2) + 2 \log^2(m_t^2 - t) - 4 \log \left( \frac{t}{t - m_t^2} \right) \log \left( \frac{m_t^2 - t}{m_t^2} \right) \right. \\ \left. + 4 li_2 \left( \frac{m_t^2}{m_t^2 - t} \right) \right\}. \quad (74)$$

$C_0^4$ ,  $C_0^8$  and  $D_0^3$  can be obtained from  $C_0^3$ ,  $C_0^6$  and  $D_0^2$  by replacing  $t$  with  $u$ .

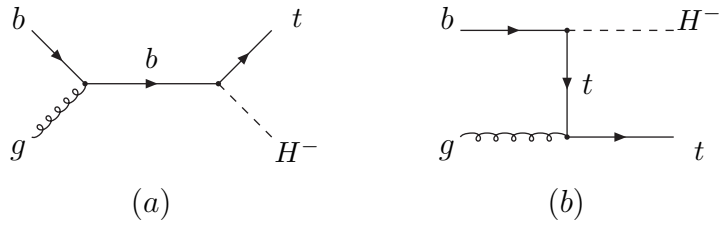


FIG. 1. Feynman diagrams at Born level of  $bg \rightarrow tH^-$ .

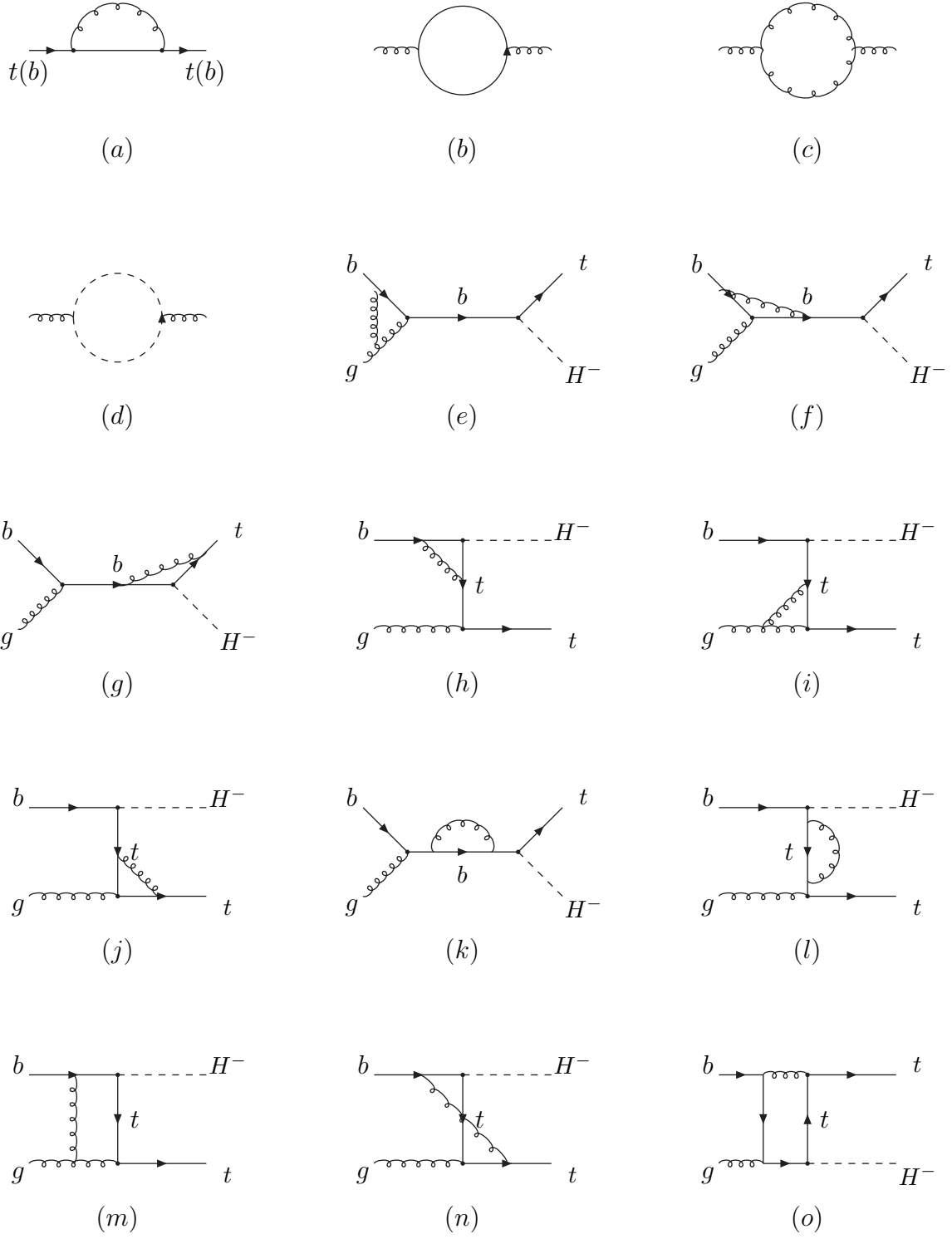


FIG. 2. Feynman diagrams of virtual contributions of  $bg \rightarrow tH^-$ .

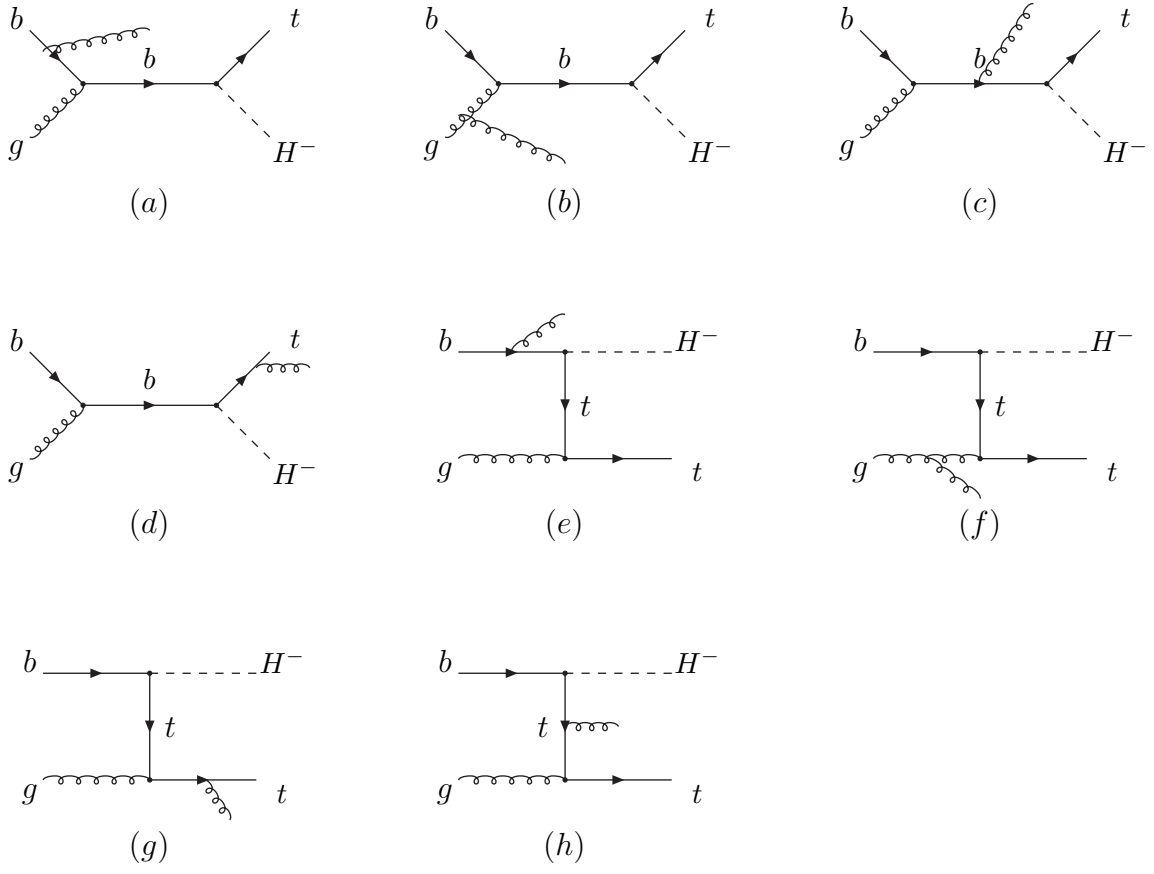


FIG. 3. Feynman diagrams of gluon-radiation process of  $bg \rightarrow tH^-g$ .

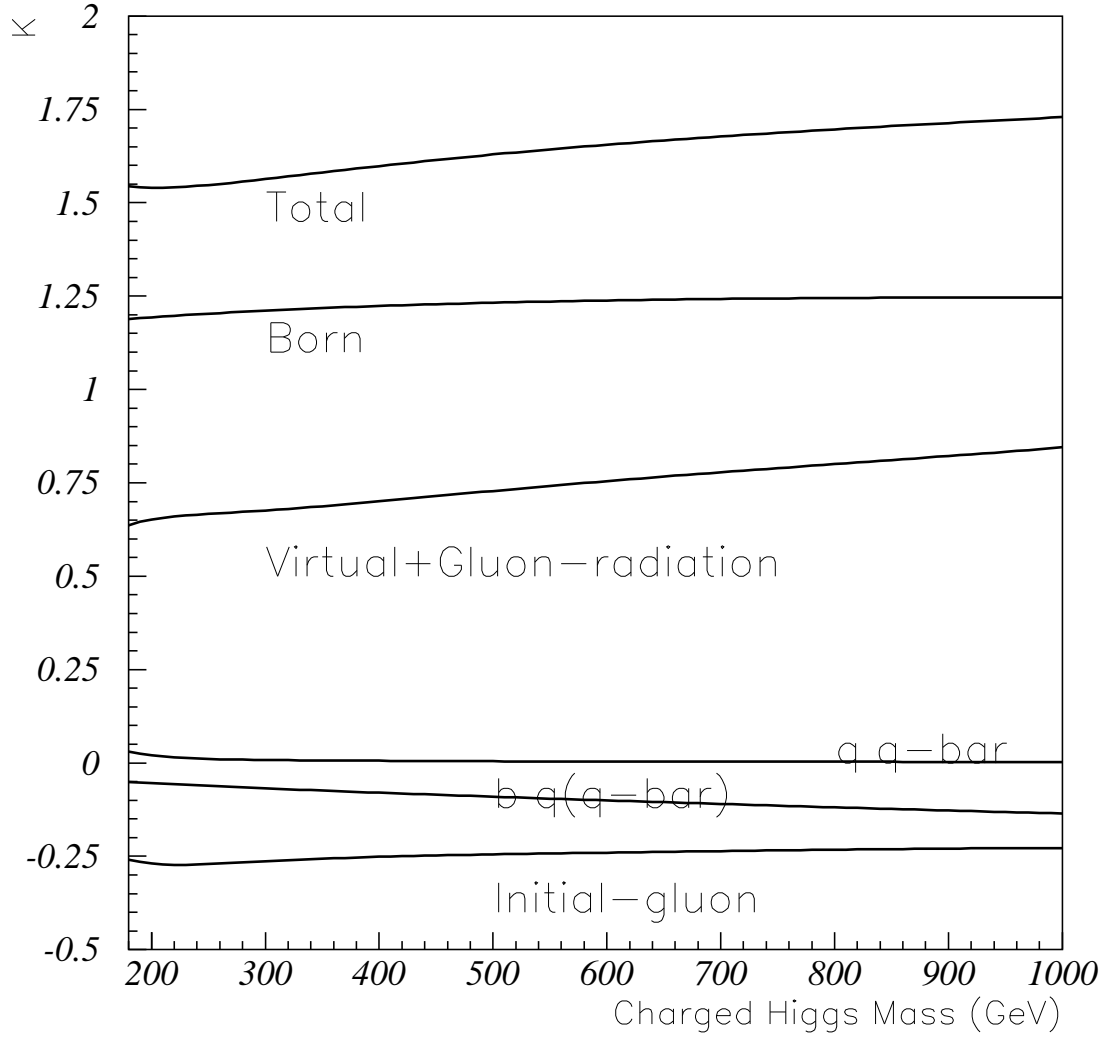


FIG. 4. The K-factors (defined in text) versus  $m_{H^\pm}$ .

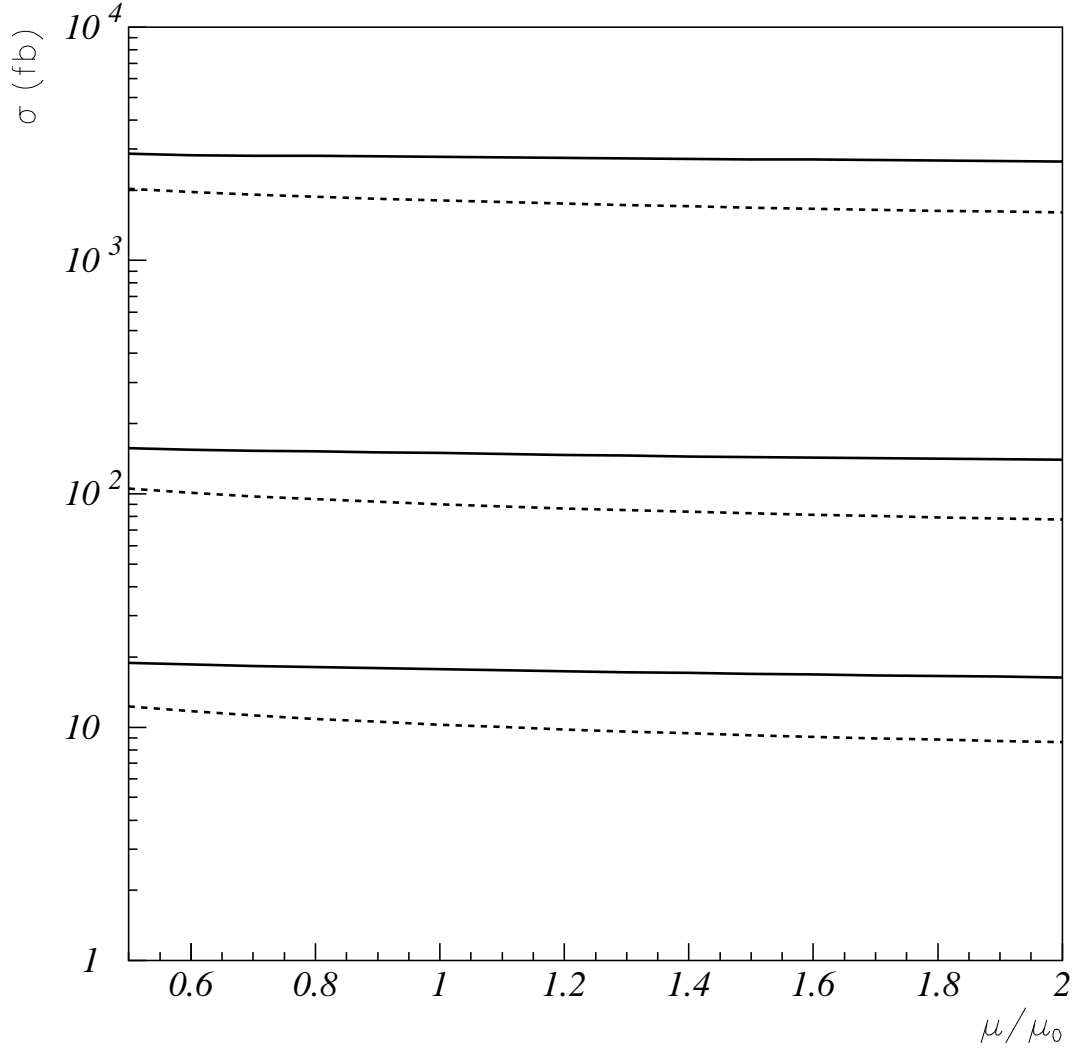


FIG. 5. Total cross sections for the process  $PP \rightarrow tH^-X$  as a function of  $\mu/\mu_0$ , where  $\mu_0 = m_{H^\pm} + m_t$ . Solid and dashed lines represent results at NLO and tree-level for  $m_{H^\pm} = 200, 600$  and 1000 GeV from top to bottom.